Breast ultrasound tomography with total-variation regularization

Cuiping Li[a], Neb Duric[b], and Lianjie Huang[c]
[a]Karmanos Cancer Institute, 4100 John R. Street, 4 HWCRC, Detroit, MI 48201; Phone: 313-576-8768, Emails: lic@karmanos.org
[b]Karmanos Cancer Institute, 4100 John R. Street, 4 HWCRC, Detroit, MI 48201; Phone: 313-576-8706, Emails: duric@karmanos.org
[c]Mail Stop D443, Los Alamos National Laboratory, Los Alamos, NM 87545; Phone: 505-665-1108; Email: ljh@lanl.gov

ABSTRACT

Breast ultrasound tomography is a rapidly developing imaging modality that that has the potential to impact breast cancer screening and diagnosis. A new ultrasound breast imaging device (CURE) with a ring array of transducers has been designed and built at Karmanos Cancer Institute, which acquires both reflection and transmission ultrasound signals. To extract the sound-speed information from the breast data acquired by CURE, we have developed an iterative sound-speed image reconstruction algorithm for breast ultrasound transmission tomography based on total-variation (TV) minimization. We investigate applicability of the TV tomography algorithm using *in vivo* ultrasound breast data from 61 patients, and compare the results with those obtained using the Tikhonov regularization method. We demonstrate that, compared to the Tikhonov regularization scheme, the TV regularization method significantly improves image quality, resulting in sound-speed tomography images with sharp (preserved) edges of abnormalities and few artifacts.

Keywords: Breast imaging, total-variation regularization, ultrasound tomography.

1. INTRODUCTION

Recent studies have demonstrated the effectiveness of ultrasound tomography imaging in detecting breast cancer[1-8]. There are basically two types of tomography methods. The first one is based on ray theory, which is fast and stable. The second one uses inverse scattering, which is much more time consuming but has relatively higher resolution[3-4,9-10]. For ray-theory based breast ultrasound tomography, there are primarily two modes. The first mode uses the time-of-flight (TOF) measurements of the transmission ultrasound signals to reconstruct the sound-speed distribution within the breast. The second one is based on attenuation measurements and reconstructs the distribution of energy absorption and scattering within the breast. This study focuses on the first mode. In most applications of ultrasound tomography to *in vivo* breast imaging, the image quality is insufficient. This is mainly due to the shortcoming of non-iterative straight-ray mathematical model employed. Based on Fermat's Principle and Snell's Law, the ultrasound ray path in an inhomogeneous medium (such as breast tissue) is not straight, which makes the inverse problem nonlinear. The first bent-ray ultrasound tomography was proposed by Schomberg in 1978[11]. However, applications of bent-ray algorithm were limited to numerical simulations and phantom studies thereafter[12-14].

To record both the transmitted and reflected ultrasound energy, a clinical ultrasound ring array scanner for breast cancer diagnosis, termed Computed Ultrasound Risk Evaluation (CURE), was designed and built at Karmanos Cancer Institute (KCI), Detroit, MI[7,8]. Since most abnormal breast lesions have higher sound-speed than normal breast tissue[15], one of the primary purposes of CURE is to be able to accurately and efficiently produce images of breast sound-speeds based on the ultrasound signals that are transmitted through the breast tissue to the other side of the ring array. Therefore, a robust ultrasound sound-speed tomography algorithm is critical to ensure a high-resolution sound-speed tomogram of the breast data.

In this study, we present an iterative bent-ray ultrasound tomography method to extract sound-speed information from *in vivo* ultrasound breast data acquired by CURE. We investigate the use of total variation (TV) to regularize the uneven ray coverage, which leads to a non-quadratic minimization problem. The TV method was introduced by Rudin et al in

Medical Imaging 2009: Ultrasonic Imaging and Signal Processing, edited by Stephen A. McAleavey, Jan D'hooge
Proc. of SPIE Vol. 7265, 726506 · © 2009 SPIE · CCC code: 1605-7422/09/$18 · doi: 10.1117/12.811044

1992, and was widely used in inverse problems in image processing (denoising, restoration and zooming) since then. While most of the regularization methods (such as Tikhonov regularization) tend to smooth reconstructed images, TV regularization preserves edge information. We apply limited memory Broyden-Fletcher-Goldfarb-Shanno (L-BFGS) method to solve the optimization problem[16], and apply the method to sixty-one *in vivo* breast datasets acquired by CURE.

2. MATERIALS AND METHODS

2.1 Data acquisition

The CURE device is a clinical prototype capable of near real time data acquisition. It is integrated into the normal patient flow of the Comprehensive Breast Center at Karmanos Cancer Institute. A detailed description of CURE was presented by Duric et al.[8] while a brief overview is given here.

The 20-cm-diameter CURE ring array consists of 256 equally-spaced and water-coupled transducers, immersed in a water tank. During the scan, the patient is positioned prone with the breast situated through a hole in the canvas bedding. The breast is suspended in water, inside the imaging tank, and encircled by the ring. A motorized gantry translates the ring in the vertical direction, starting from the chest wall through the breast nipple region. One complete scan takes approximately 1 minute, and consists of 50-80 slices of data per patient depending on the size of the breast.

During scanning at each step, each of 256 transducer elements sequentially emits a fan beam of ultrasound signals with a central frequency of 1.5 MHz toward the opposite side of the ring. The forward scattered (transmission) and backscattered (reflection) ultrasound signals are subsequently recorded by all 256 elements at a sampling rate of 6.25 MHz. The data are used to reconstruct images of acoustic properties.

2.2 Ultrasound Sound-speed Tomography

Based on the Radon transform, classical tomography reconstruction using filtered back-projection (FBP) cannot take ray bending into account. However, according to Fermat's Principle and Snell's Law, the ultrasound ray path in an inhomogeneous medium (such as breast tissue) is not straight, which makes the inverse problem nonlinear. We study an iterative bent-ray ultrasound tomography algorithm with a TV regularization term for ultrasound transmission sound-speed tomography. To solve the bent-ray ultrasound tomography problem, a regular rectangular grid model is created on the image plane, whose boundaries enclose the transducer ring. During each iteration, both the forward problem and the inverse problem are solved, and the sound-speed model is updated for the successive iterations. Details about our methods to solve forward and inverse problems are described in the following.

Forward Modeling

2-D ultrasound wave propagation is governed by the eikonal equation

$$(\nabla E)^2 = (\partial T/\partial x)^2 + (\partial T/\partial y)^2 = (1/v)^2 = (s_x^2 + s_y^2), \quad (1)$$

where T is the travel-time, v is the sound-speed, and (s_x, s_y) is the slowness vector of the ultrasound wave that is defined as the inverse of the sound speed. In eq. (1), $E = const.$ describes the 'wavefronts', and 'rays' are defined as the orthogonal trajectories of these wavefronts.

In this paper, eq. (1) is solved using Klimes' grid travel-time tracing technique (1996), which has been proven to be both accurate and computationally efficient. Klimes' method calculates the slowness vector (s_x, s_y) and travel-time T at the center point of each grid cell simultaneously with at least second-order accuracy in space. (s_x, s_y) and T at an arbitrary point within the grid model are interpolated by a 2-D fourth-order Lagrange interpolation algorithm. An ultrasound ray is backprojected from a receiver to the transmitter in the following way:

(1) Starting from the receiver location (x_r, y_r), the ray segment within the current grid cell istraced along the direction $\bar{G} = (-s_{x_r}, -s_{y_r})$ until it intercepted the cell boundary at point (x_i, y_i);

(2) Update $\bar{G}$ to be the negative slowness vector of the intercept point $\bar{G} = (-s_{x_i}, -s_{y_i})$, and trace the ray segment within the next adjacent cell;
(3) Repeat (2), until the current ray reaches the transmitter within a certain tolerance.

Assuming that the slowness is constant within each grid cell, the bent ray path can be traced using the above procedure accurately.

Inverse Problem

Let Δt_i be the difference between the i^{th} picked time-of-flight for the recorded ultrasound data and the i^{th} calculated TOF for the sound-speed model, our inverse problem can be described as follows

$$\sum_j^M l_{ij} \Delta s_j = \Delta t_i \,, \tag{2}$$

where Δs_j is the slowness perturbation for the j^{th} grid cell, which needs to be inverted, and l_{ij} is the ray length of the i^{th} ray within the j^{th} cell. Equation (2) can be expressed as a matrix form

$$L\Delta S = \Delta T \,. \tag{3}$$

This is a nonlinear inverse problem due to ray bending. The objective function for the inverse problem can be described as in eq. (4)

$$f = \arg\min_{\Delta S}(\| L\Delta S_\lambda - \Delta T \|^2 + \lambda TV(\Delta S_\lambda)) \,, \tag{4}$$

with

$$TV(\Delta S_\lambda) \equiv \iint \sqrt{|\nabla(\Delta S_\lambda)|^2}\, dxdy \,. \tag{5}$$

However, $TV(\Delta S_\lambda))$ is not differentiable at zero. To avoid this problem, a small positive constant value is added to the equation (6)

$$TV(\Delta S_\lambda) = \iint \sqrt{|\nabla(\Delta S_\lambda)|^2 + \beta^2}\, dxdy \,. \tag{6}$$

The quantity $\sqrt{|\nabla(\Delta S_\lambda)|^2 + \beta^2}$ is known as the gradient magnitude. This provides us with the information about the discontinuities in the image. In eq. (4), λ is the regularization parameter that balances the roughness of the inverted results and the fit to the data.

To avoid direct computation of Hessian matrices, we apply the quasi-Newton algorithm—limited memory Bryoyden-Fletcher-Goldfarb-Shanno (LBFGS) method to iteratively solve the nonlinear problem in eq. (4) for ΔS, starting with a homogeneous sound-speed model (algorithm available at: http://www.alglib.net/optimization/lbfgs.php). The LBFGS method has been proven to be both time and memory efficient[16]. After each iteration, an updated sound-speed model is obtained by adding the solution ΔS to the initial model. Rays are traced on the updated model using the method discussed in the forward modeling section, and the TOF data are updated at the same time. The iteration continues until the TOF misfit ΔT is not longer significantly improved from the previous iteration, which means the solutions have converged. The regularization parameter λ is determined using L-curve technique (refer to Hansen's paper for details, available at http://www.math/sintef.no/vskoler/2005/notes/Lcurve.pdf).

3. RESULTS

We apply our TV tomography algorithm to a total of 61 *in vivo* breast datasets. Uncertainties in the sound-speed tomograms are simply estimated by calculating the standard deviation in reconstructions for water shot data. Water shot data are recorded right before each patient scan, with only water in the tank. Sixteen reconstructions with 1 mm by 1 mm grid cell for water shot data are used to do the analysis. The typical standard deviation for the sound-speed values in water is 4 *m/s* per pixel.

Our clinical protocol is designed to include a sample of patients with a wide variety of breast types, ranging from fatty to dense on the BI-RADS categories 1-4. The sound-speed tomograms are reviewed and classified by radiologists.

3.1 Total-variation (L_1-norm)) regularization vs. Tikhonov (L_2-norm) regularization

We compare the TV sound-speed tomograms (with three iterations) to those reconstructed with the classic Tikhonov regularization (also with three iterations). One example is presented in Fig. 1, where (a)-(c) are TV tomogram, Tikhonov tomogram, and sound-speed cross-sections along the solid in (a) (upper panel) and along the dashed line in (b) (lower panel), respectively. The breast in Fig. 1 has a 55 x 47 x 37 mm invasive ductal carcinoma at 12:00 to 1:00 o'clock. Note that the TV method not only preserved sharper edges of the lesion, but also damped out the "ray" artifacts much better than the Tikhonov method. Two tomograms in Fig. 1 are shown in the same absolute sound-speed scale ranging from 1350 m/s to 1600 m/s.

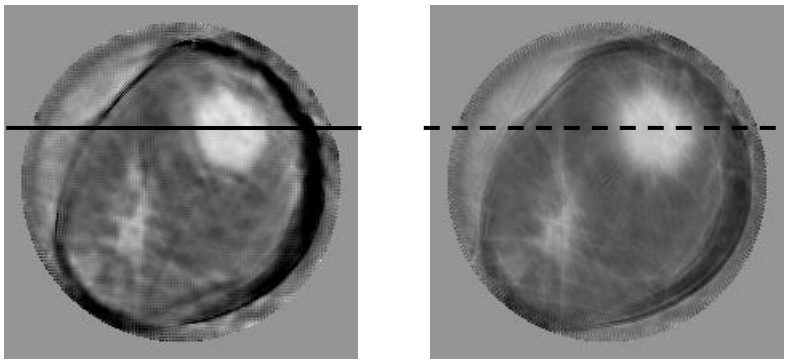

(a) TV reconstruction (b) L_2-norm reconstruction

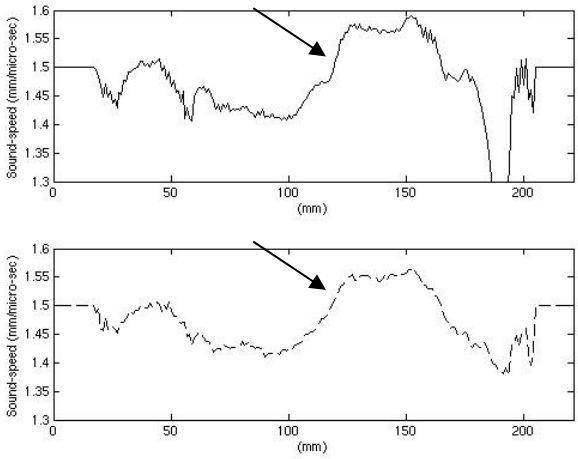

(c) Cross sections along the solid line in (a) and dashed line in (b)

Figure 1.Comparison of TV (L_1-norm) reconstruction in (a) with classic Tikhonov (L_2-norm) reconstruction in (b). The breast has a 55 x 47 x 37 mm invasive ductal carcinoma at 12:00-1:00 o'clock. The sound-speed scale in (a) and (b) is from 1350 m/s to 1600 m/s. Figures in (c) show cross sections along the solid line in (a) (upper panel) and the dashed line in (b) (lower panel). The arrows point to the locations where the TV reconstruction preserves a better/sharper edge of the lesssion.

3.2 Bent-ray inversion vs. straight-ray inversion

We also compared TV bent-ray sound-speed tomograms for in vivo data with their straight-ray counterparts. Our analysis shows that, for our selected patients, the bent-ray approach led to sharply improved image quality. An *in vivo* example is used to illustrate this improvement.

Figure 2 is an example demonstrating the improvements of the TV bent-ray reconstruction over a straight-ray reconstruction. Figure 2a is the TV bent-ray inversion (third iteration), Fig. 2b is a straight-ray inversion result, and (c) is sound-speed cross-sections along the solid line in 2a (upper panel) and the dashed line in 2b (lower panel). The arrows indicate the lesion location. According to clinical examinations (mammogram, ultrasound and pathology), the breast shown in Fig. 2 has a 1.6 x 1.1 x 1.8 cm big fibroadenoma at 2:00 o'clock. Our radiologist is able to pick it up in the TV bent-ray image (indicated by the arrow in Fig. 2a), while it is much less obvious in the straight-ray inversion (Fig. 2b). Both the TV bent-ray tomogram and the straight-ray tomogram in Fig. 2 are shown in the same absolute sound-speed scale from 1350 m/s to 1550 m/s. Sound-speeds of the lesions are also illustrated in their cross sections (Fig. 2c) where the lesions are indicated by the arrows.

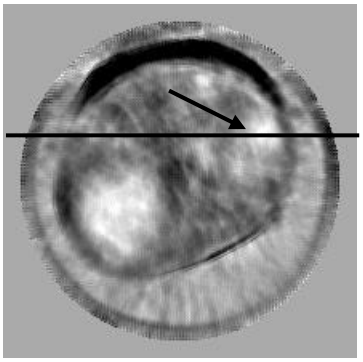

(a) Sound-speed tomograms using bent-ray algorithm (third iteration).

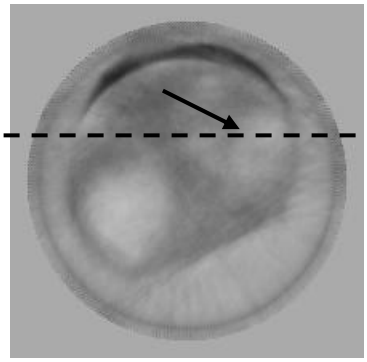

(b) Sound-speed tomograms using straight-ray algorithm.

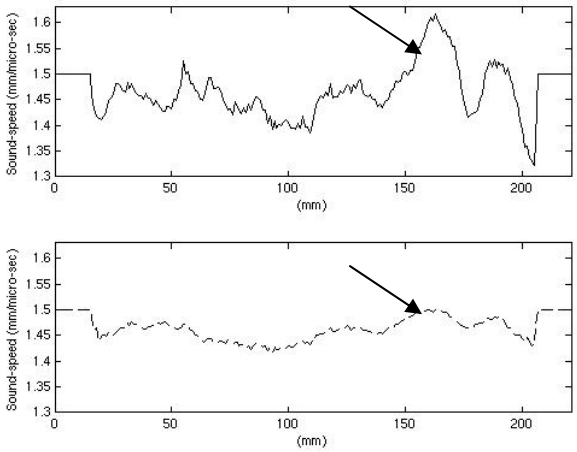

(c) Cross sections along the solid line in (a) and dashed line in (b).

Figure 2. Sound-speed tomograms for a dense breast with a 16 x 11 x 18 mm fibroadenoma at 2:00 o'clock. The sound-speed scale in (a) and (b) is from 1350 m/s to 1550 m/s. Cross sections in (c) demonstrate that the TV reconstruction method give a clear high-sound-speed lesion that is not clearly shown in the straight-ray inversion result.

3.3 Fatty tissue vs. breast parenchyma

Breast density is a known risk factor for developing breast cancer. Breast density is determined by the ratio of breast parenchyma to fatty tissue within the breast. Separation of fatty tissue from breast parenchyma would be a significant step for breast density evaluation using our sound-speed tomograms. Examples of sagittal views of four breasts within the BI-RAD categories 1-4 are presented in Fig. 3, where the breast parenchyma (in light color) is clearly discernible from fatty tissue (in dark color). These sagittal sound-speed tomograms are generated by reslicing the coronal sound-speed stacks in ImageJ, and illustrated in the same absolute sound-speed scale from 1350 m/s to 1550 m/s.

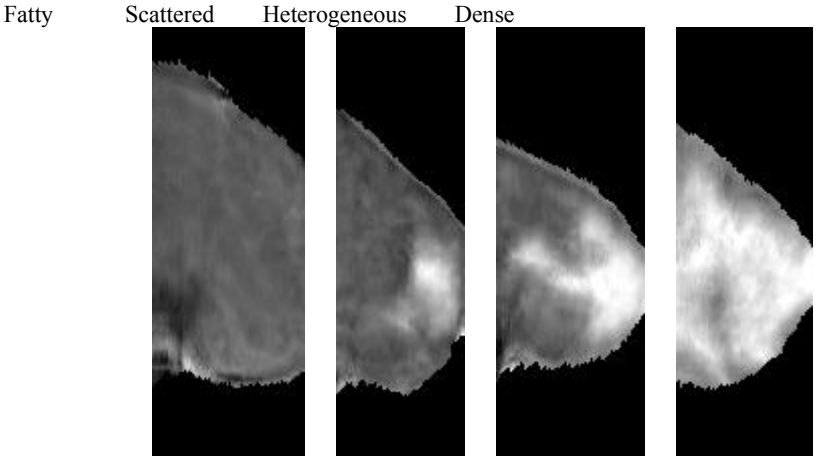

Figure 3. Sagittal views constructed from our sound-speed image stacks, for breasts of different densities corresponding to BI-RADS categories 1-4 from the left panel to the right panel. All figures are shown in the same absolute sound-speed scale from 1350 m/s to 1550 m/s

We utilize the k-mean clustering routine of ImageJ (an open source package available at http://rsb.info.nih.gov/ij) to segment every 10th sound-speed tomogram for each patient. Since the abnormal lesions are not considered part of the normal breast architecture, we remove them from the sound-speed tomograms before we apply the clustering. Details of k-mean clustering segmentation are described by Glide et al.[17]. For more quantitative comparison, we calculate the mean sound-speeds for fatty tissue and breast parenchyma based on these segmentation results. The calculated mean sound-speeds are $1422 \pm 9 m/s$ (mean $\pm$ SD) and $1487 \pm 21 m/s$ for fatty tissue and breast parenchyma, respectively (Table 1).

Table 1. Mean sound-speed with standard deviation (SD).

	Sound-speed (m/s)
Fat	1422 ± 9
Parenchyma	1487 ± 21
Malignant mass	1548 ± 17
Benign mass	1513 ± 27

3.4 Benign vs. malignant lesions

Of 32 lesions in 61 patients, 19 are malignant (16 invasive ductal carcinoma (IDC) and 3 ductal carcinoma in situ (DCIS)) and 13 are benign (8 fibroadenoma and 5 cyst, complicate cyst or fibrocystic structure). We select the slices that contain lesions based on radiologists' evaluations, and isolate the lesions by either referring to reflection images or thresholding.

The mean sound-speed of lesion for a single patient is calculated by summing all sound-speeds for every pixel within ROI in the selected slices, then dividing this summation by the total number of pixels. Mean sound-speed histograms for 13 benign lesion and 19 malignant lesions are depicted in Fig. 4, where malignant lesions show, on average, higher mean

sound-speed than benign lesions. The mean sound-speeds for malignant and benign lesions are $1548 \pm 17\ m/s$ and $1513 \pm 27\ m/s$, respectively. Our results generally corresponded with those reported in literature. Duck[18] has calculated the mean sound-speeds for carcinoma and fibroadenoma to be $1584 \pm 27\ m/s$ and $1550 \pm 32\ m/s$, respectively. Chang[19] reports a mean sound-speed of $1499.8 \pm 26.8\ m/s$ for fibroadenoma and a mean sound-speed of $1530.9 \pm 36.2\ m/s$ for carcinoma.

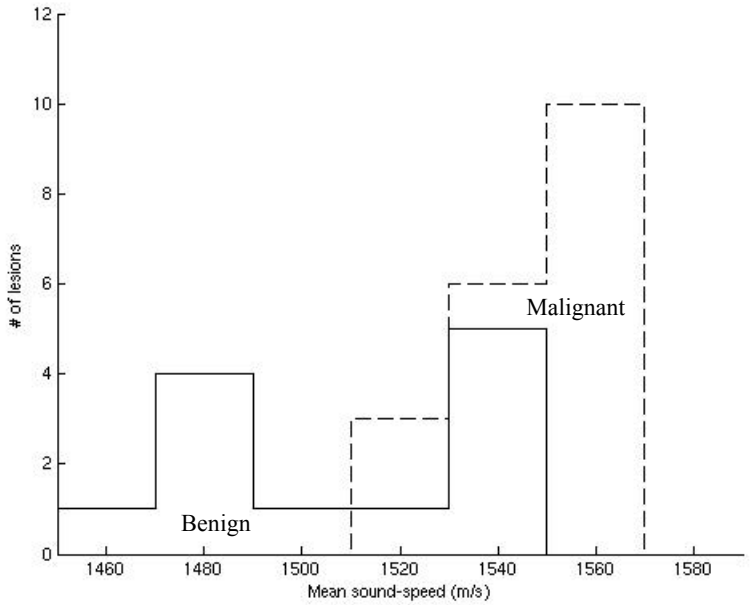

Figure 4. Histogram of mean sound-speeds for 13 benign lesions (solid line) and 19 malignant lesions (dashed line).

4. DISCUSSION AND CONCLUSIONS

We have developed a total-variation-based bent-ray tomography algorithm for imaging sound-speed distribution of the breast. We have applied this algorithm to 61 breast datasets acquired using a clinical prototype CURE with a ring transducer array. Our *in vivo* results clearly demonstrate that the TV reconstruction is superior to the reconstruction obtained with the classic Tikhonov regularization. Although TV is computationally more expensive than Tikhonov reconstruction, Vogel et al[20] have demonstrated that the difference in computational expense between the two methods is not significant. Our TV reconstruction takes almost the same computational time as the Tikhonov reconstruction. In

We have shown that fatty and dense tissues could be well separated in our sound-speed images. The mean sound-speed of malignant lesions, on average, is higher than that of benign ones.

The results of our study suggest some potential clinical applications for our bent-ray tomography algorithm. First, our sound-speed tomograms may be used to assess breast density. The positive correlation between mean sound-speed and breast mammographic density makes it possible to use mean sound-speed to evaluate breast density, and consequently to assess breast cancer risk. Second, sound-speed images can help to detect and characterize breast lesions. Fusing sound-speed images with the corresponding attenuation and reflection images may help differentiate benign from malignant breast lesions.

ACKNOWLEDGEMENTS

The authors wish to thank Lisa Bey-Knight for her help in recruiting patients and data collection. C. Li also wants to acknowledge Jason Shen for his assistance for the ROI segmentation of our images. This work was supported in part by

a research grant from the Michigan Economic Development Corporation (MEDC) and Susan G. Komen Breast Cancer Foundation. L. Huang acknowledges the support of the U.S. DOE Laboratory-Directed Research and Development program at Los Alamos National Laboratory.

REFERENCES

1. Carson, P. L., Meyer, C. R., Schezinger, A. L., and Oughton, T. V., "Breast imagin in coronal planes with simultaneous pulse echo and transmission ultrasound," Science 214,1141-1143 (1981).
2. Andre, M. P., Janee, H. S., Martin, P. J., Otto, G. P., Spivey, B. A., and Palmer, D. A., "High-speed data acquisition in a diffraction tomography system employing large-scale toroidal arrays," International Journal of Imaging Systems and Technology 8, 137-147 (1997).
3. Johnson, S. A., and Tracy, M. L., "Inverse scattering solutions by a sinc basis, multiple source, moment method—part I: Theory," Ultrason. Imaging 5, 361-375 (1983).
4. Johnson, S. A., Borup, D. T., Wiskin, J. W., Natterer, F., Wuebbling, F., Zhang, Y., and Olsen, C., "Apparatus and Method for Imaging with Wavefields using Inverse Scattering Techniques," United States Patent 6,005,916 (1999).
5. Marmarelis, V. Z., Kim, T., and Shehada, R. E., "High-resolution ultrasound transmission tomography", Proc. SPIE Medical Imaging, 5035, paper 6, 2003.
6. Liu, D. L., and Waag, R. C., "Propagation and backpropagation for ultrasonic wavefront design," IEEE Trans. on Ultras. Ferro. and Freq. Contr. 44, 1-13 (1997).
7. Duric, N., Littrup, P. J., Babkin, A., Chambers, D., Azevedo, S., Kalinin, A., Pevzner, R., Tokarev, M., Holsapple, E., Rama, O., and Duncan, R., "Development of Ultrasound Tomography for Breast Imaging: Technical Assessment," Medical Physics 32, 1375–1386 (2005).
8. Duric, N., Littrup, P., Poulo, L., Babkin, A., Pevzner, R., Holsapple, E., Rama, O., and Glide, C., "Detection of breast cancer with ultrasound tomography: First results with the Computed Ultrasound Risk Evaluation (CURE) prototype," Medical Physics 34, 773-785 (2007).
9. Devaney, A., "Inverse scattering theory within the Rytov approximation," Opt. Lett. 6, 374-376 (1981).
10. Devaney, A., "Inverse formula for inverse scattering within the Born approximation," Opt Lett. 7, 111-112 (1982).
11. Schomberg, H., "An improved approach to reconstructive ultrasound tomography," J. Phys. D: Appl. Phys 11, L181-L185 (1978).
12. Norton, S.J., "Computing Ray trajectories between two points: A solution to the ray-linking problem," Optical Society of America 4, 1919-1922 (1987).
13. Andersen, A.H., "Ray linking for computed tomography by rebinning of projection data," J. Acoust. Soc. Am. 81, 1190-1192 (1987).
14. Andersen, A.H., "A ray tracing approach to restoration and resolution enhancement in experimental ultrasound tomography," Ultrasound Imaging 12, 268-291 (1990).
15. Gauss, R. C., Soo, M. S., and Trahey, G.E., "Wavefront distortion measurements in the human breast," IEEE Ultraon Sympos 2, 1547-1551 (1997).
16. Nocedal, J., and Wright, S. J., "Limited-Memory Quasi-Newton Methods: Numerical Optimization," Springer, 2nd ed. New York: Mikosch TV, Resnich SI, Robinson SM (2000).
17. Glide, C. K., Duric, N., and Littrup, P., "Novel approach to evaluating breast density utilizing ultrasound tomography," Medical Physics 34, 744-753 (2007).
18. Duck, F. A., "Physical properties of tissue," London: Academic Press (1990).
19. Chang, C. H., Huang, S. W., Yang, H. C., Chou, Y. H., and Li, P. C., "Reconstruction of ultrasonic sound velocity and attenuation coeeficient using linear arrays: clinical assessment," Ultrasond in Med. & Biol. 33, 1681-1687 (2007).
20. Vogel, C. R., and Oman, M. E., Fast, "Robust Total Variation-Based Reconstruction of Noisy, Blurred Images," IEEE Transactions on Image Processing 7, 813-824 (1998).